21st IAEA Fusion Energy Conference
Chengdu, China, 16 - 21 October, 2006

IAEA-CN-149/ EX/P1-14

Steady-State Operation of ICRF Heated Plasma in the Large Helical Device

T. Mutoh et al.

NIFS-844 Oct. 2006

Steady-State Operation of ICRF Heated Plasma in the Large Helical Device

T.Mutoh 1), R.Kumazawa 1), T.Seki 1), K.Saito 1), H.Kasahara 1), Y.Nakamura 1), S.Masuzaki 1), S.Kubo 1), Y.Takeiri 1), T.Shimozuma 1), Y.Yoshimura 1), H.Igami 1), T.Watanabe 1), H.Ogawa 2), J.Miyazawa 1), M.Shoji 1), N.Ashikawa 1), K.Nishimura 1), M.Osakabe 1), K.Tsumori 1), K.Ikeda 1), K.Nagaoka 1), Y.Oka 1), H.Chikaraishi 1), H.Funaba 1), S.Morita 1), M.Goto 1), S.Inagaki 1), K.Narihara 1), T.Tokuzawa 1), R.Sakamoto 1), T.Morisaki 1), B.J.Peterson 1), K.Tanaka 1), H.Nakanishi 1), M.Nishiura 1), T.Ozaki 1), F.Shimpo 1), G.Nomura 1), C.Takahashi 1), M.Yokota 1), Y.P.Zhao 3), J.G.Kwak 4), S.Murakami 5), H.Okada 5), H.Yamada 1), K.Kawahata 1), N.Ohyabu 1), O.Kaneko 1), K.Ida 1), Y.Nagayama 1), K.Y.Watanabe 1), N.Noda 1), A.Komori 1), S.Sudo 1), O.Motojima 1)

1) National Institute for Fusion Science, Oroshi-cho 322-6, Toki city, 509-5292, Japan
2) Graduate University for Advanced Studies, Hayama, 240-0163 Japan
3) Institute of Plasma Physics, Academia Sinica, Hefei, 230031, P.R.China
4) Korea Atomic Energy Institute, Daejeon,305-600, Korea
5) Kyoto University, Kyoto 606-8501, Japan

e-mail contact of main author: mutoh@nifs.ac.jp

Abstract. Achieving steady-state plasma operation at high plasma temperatures is one of the important goals of worldwide magnetic fusion research. High temperatures of approximately 1-2 keV, and steady-state plasma-sustainment operations have been reported. After the last IAEA conference, the steady state operation regime was greatly extended in the Large Helical Device (LHD). A high-temperature plasma was created and maintained for more than 30 min with a world record injected heating energy of 1.3 GJ in 2004FY, and recently for 54 min with 1.6 GJ in the 2005FY experimental program. The three-dimensional heat-deposition profile of the LHD helical divertor was modified, and during long-pulse discharges it effectively dispersed the heat load using a magnetic-axis swing technique developed at the LHD. A sweep of only 3 cm in the major radius of the magnetic axis position (less than 1% of the major radius of the LHD) was enough to disperse the divertor heat load. The steady-state plasma was heated and sustained mainly by hydrogen minority ion heating using ion cyclotron range of frequencies (ICRF). By accumulating the small flux of charge-exchanged neutral particles during the long pulse operation, a high energy ion tail which extended up to 1.6 MeV was observed. The long pulse operations lasted until a sudden increase of radiation loss occurred, presumably because of metal wall flakes dropping into the plasma. The sustained line-averaged electron density and temperature were approximately 0.8×10^{19} m^{-3} and 2 keV, respectively, at a 1.3GJ discharge (#53776) and 0.4×10^{19} m^{-3} and 1 keV at a 1.6GJ discharge (#66053). The average input power was 680 kW and 490 kW, and the plasma duration was 32 min and 54 min, respectively. These successful long operations show that the heliotron configuration has a high potential as a steady-state fusion reactor.

1. Introduction

The Large Helical Device (LHD) is the world's largest superconducting fusion device, having continuous helical coils of $l = 2$ and $m = 10$ [1]. A magnetic field of 3 T is available for steady-state operation. Its nominal major and minor radii are 3.9 m and 0.6 m, respectively. A number of physical and technological topics using the LHD have been studied and reported [2-4]. One of the main missions of the LHD is to develop the physics and technology for long-pulse or steady-state operation using an intrinsic helical divertor [5, 6]. This mission is well suited to the LHD, because a heliotron device does not require an internal plasma current for plasma confinement; it is also a superconducting steady-state device.

The structure of the magnetic configuration of the LHD is quite different from axisymmetric toroidal devices such as tokamaks, especially with regard to the outer region of the last closed flux surface. The LHD contains no clear separatrix, and the structure is characterized by the coexistence of a

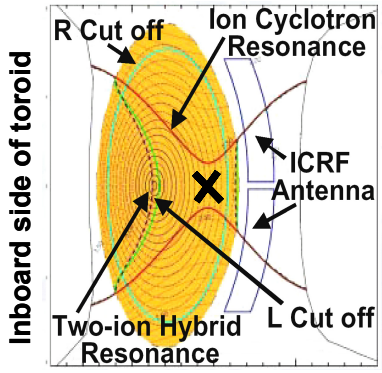

FIG. 1. Resonance and cutoff surfaces on the cross section of LHD plasma at the vertically elongated section are shown. (Helium plasma with minority hydrogen: $n_H/(n_H+ n_{He})$ = 30 %, center electron density: $n_{e0} = 1.0 \times 10^{19}$ m^{-3}, magnetic field strength: B_0 = 2.75 T, magnetic axis radius: R_{ax} = 3.6 m, frequency: 38.47 MHz, $k_{//} = 5$ m^{-1})

stochastic region, residual islands, whisker structure, a laminar region, and the intrinsic helical divertor. The helical divertor in the LHD has four divertor legs [7]. The distribution of the particle and heat loads along the divertor traces is not uniform, and the distribution pattern can be significantly changed by small changes of the magnetic axis position [5]. It has been reported that during the long plasma operation period, the magnetic axis was slowly swung reciprocally in order to disperse the heat load along the divertor traces, and the maximum temperature of the carbon divertor plates was greatly reduced. This technique was first introduced in the LHD in the 2004FY experimental program [8, 9].

Steady-state operation was attempted in the LHD over a period of six years using various heating devices: neutral beam injection (NBI), electron cyclotron (ECH), and ion cyclotron range of frequencies (ICRF). The steady-state operation of the heating device is quite a difficult undertaking because the plasma-heating device was designed for high-power, short-pulse operation at critical capacity. It is not optimized for long-pulse operation. Recently, ECH heating devices [10, 11] and ICRF [12, 13] have been developed for long-duration operation. In the previous two-year experimental programs we used both ECH and ICRF devices as continuously operating devices and NBI for periodic pulse operation. The successful long-pulse operation was undertaken to provide an understanding of the physics of divertor heating, device development, and innovative magnetic field operation techniques.

Before the LHD experiment, several tokamak devices had shown excellent performance in long-pulse experiments. Tore Supra achieved 6 min operation at 1.07 GJ [14, 15], TRIAM-1M achieved 5 hour operation [16], and JT-60U achieved 65 s operation [17], all using the lower hybrid current drive (LHCD) technique. The requirement of a current drive effort to perform long plasma operation is the largest difference between heliotron devices and tokamaks.

2. Steady-State Plasma Operation Using ICRF and EC Heating

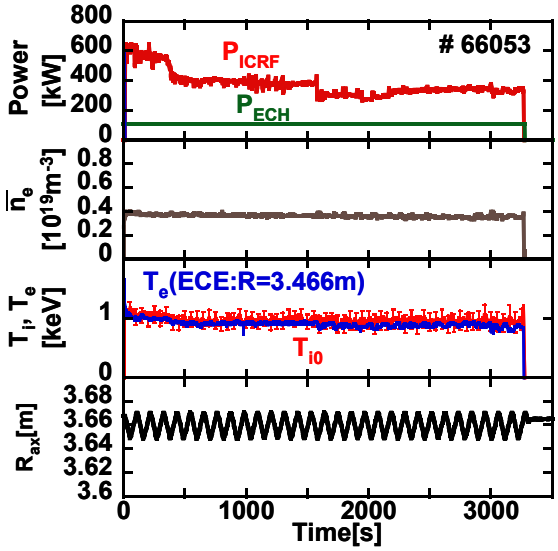

FIG. 2. Plasma parameters of the 54 min operation with 1.6 GJ input energy: input power of ICRF and ECH, line-averaged electron density, ion and electron temperature and magnetic axis radius (reciprocally swept)are shown. (He(H:minority), 2.75 T at R = 3.6 m)

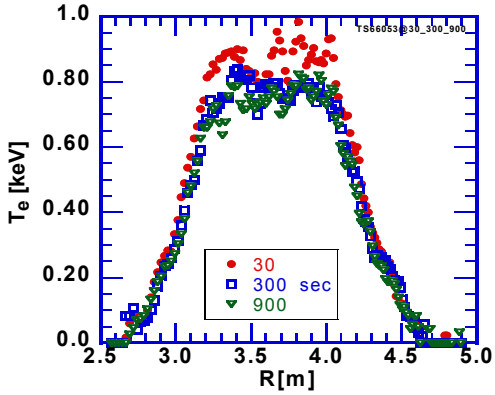

FIG. 3. Electron temperature profiles measured by Thomson scattering at various timings on 54 min operation. (#66053)

ICRF antennas are installed on the outer side of the torus at the vertically elongated sections [12]. For steady-state operation of the LHD, six antenna loops were installed and four antennas were connected to transmitters through specially developed ceramic feed-throughs, coaxial lines, and liquid impedance tuners. The ICRF resonance

and cutoff layers in the plasma cross section are shown in Figure 1. The ICRF heating mode for the long-pulse experiment used minority heating with helium as the majority ions and hydrogen as the minority ions [18-21]. Around the saddle point (marked as X in the figure), the gradient of the magnetic field is very small. Strong cyclotron damping can be expected if the cyclotron resonance is located near the saddle point, as shown in the figure. Good ICRF-heating performance was obtained with this resonance location. The left-hand cut-off, and the two-ion hybrid resonance layers were located near the plasma axis for a majority helium concentration of 70% and minority proton concentration of 30%.

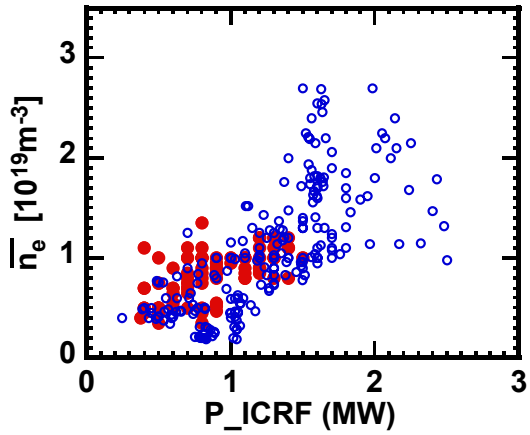

FIG. 4. Line averaged electron density of ICRF maintained plasmas are plotted versus input power. Large solid marks are long pulse discharge for more than 1 min and small marks are data of short pulse plasma less than 10 sec.

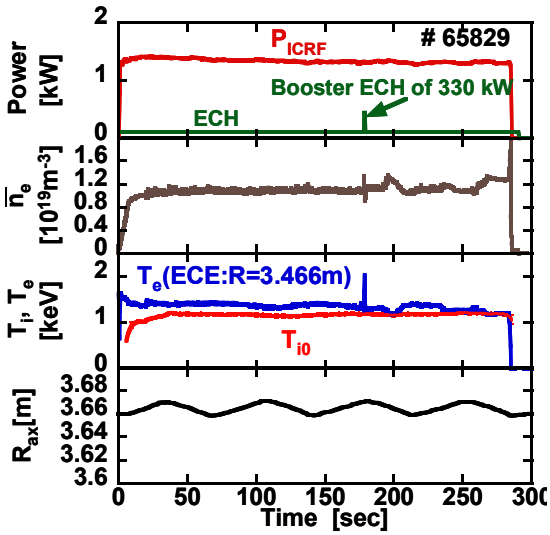

FIG. 5. Plasma parameters of higher density and higher power operation during 5 min. Booster ECH pulse of 0.6 sec duration was additively injected by event trigger system when metal impurity flake was dropped into plasma.

Subsequent to the experimental program of 2003, a continuous wave (CW) ECH system began operation at the LHD. It successfully operated for 12 min with 100 kW injection power in the 2003FY experimental program [11]. The ECH system was also improved, especially the transmission-line system, for a longer operation program. In the 2004FY experimental program, the ECH 110 kW CW system and the ICRF 1MW CW system could be used simultaneously. In the 2004FY program, the ECH was able to sustain the plasma for more than 1 hour at a power level of 110 kW, which is the duration record for plasma sustainment at the LHD. The frequency of the ECH is 84 GHz, it resonates at 3 T, and the cyclotron-resonant layer is not on the plasma axis but at approximately 0.4 times the radius of the plasma. For the 30 min operation (shot no. 53776), repetitive NBI heating of 500 kW with 25 s pulses was also used as the auxiliary heating device [22]. In this operation, the averaged input power was 680 kW and the input energy to the plasma was 1.3 GJ.

The LHD vacuum chamber was conditioned by boronization, which was effective in keeping the impurity influx at low levels during steady-state operation.

In the 2005FY program, extension of the steady state operation region was attempted using ICRF and EC heating. A successful result was achieved by controlling the input power level during the operation as a way to suppress the arcing which was main cause of sudden impurity influx from the chamber wall or divertor carbon plates. The temporal behavior of 54 minutes operation is shown in Figure 2. The ICRF and ECH were injected continuously. The input heating power was gradually decreased and the average power was 380 kW for ICRF and 110 kW for ECH. The total input energy to the plasma reached 1.6 GJ. The ICRF power was manually decreased to reduce occasional metal impurity influx. The line-averaged electron density was 0.4 x 10^{19} m^{-3} and electron and ion temperatures were around 0.8 to 1 keV. The magnetic axis position was reciprocally swept between 3.65m and 3.67 m in order to disperse the divertor heat load effectively. The electron temperature profiles are shown in Figure3. The profiles are flat and not notably peaked. On the ICRF heating, the bulk heating power was due mainly to collisional relaxation by the high energy minority ions. In this parameter range, the ion temperature is a little higher than the electron temperature. The power deposition profiles of the ICRF and the ECH are expected to be broad in the core plasma region.

Figure 4 shows the plasma density region using ICRF heating only. The large red marks indicate the data of long pulse operations for more than 1 minute, while the small open marks correspond to the

short pulse operations of 2 to 10 second duration. In the higher plasma density region, the energy confinement time and the ICRF heating efficiency increase. Therefore, parameters such as fusion triplet are increased with increases in plasma density. To sustain the higher density plasma, the required power was large, as shown in Figure4. At the higher power operation, the flakes of impurity metal dropped more frequently. This event restricted the plasma operation duration. The mitigation of local heat load is one of the key factors. This point is discussed in the next section. Another direct action to sustain the plasma against the sudden radiation collapse is the newly developed booster ECH injection.

Plasma of higher power and the higher density is shown in Figure 5. The ICRF power was around 1.3 MW and the plasma density was around 1.1 x 10^{19} m^{-3}. At 178 sec, a block of impurity metal dropped into the plasma and the density increased suddenly. Typically, plasma is collapsed by the radiation loss caused by such an increase. In this shot, an additional ECH pulse of 330 kW was injected during 0.6 sec which was triggered at the sudden increase of the FIR interferometer signal. A booster ECH pulse has the effect of recovering the electron temperature and also suppressing the plasma density during the ECH heating. The booster ECH system has to wait for 3 minutes to restart as the next pulse; therefore, only one pulse was available in this operation because the next impurity influx occurred after 2 minutes. This technique will be useful for future long pulse operations.

3. Heat-Load Characteristics and Magnetic-Axis Swing Operation

In the heliotron configuration, the intrinsic divertor structure is formed without any additional coils [7]. The stochastic regions exists near the last closed flux surface (LCFS). The field lines in this region approach the LCFS, and are the main channel for particle and heat transport from the LCFS to the divertor [5]. The magnetic structure in the SOL and the divertor are different for toroidal and poloidal locations; that is, the structure is three-dimensional. The essential factor determining the profiles for particle and heat loads on the divertor is the local shear of the rotational transform near the residual X-points [6]. This is determined by the operational magnetic configuration, such as the major radius of the magnetic axis (R_{ax}). For the case of R_{ax} = 3.6 m, the divertor legs are thicker at the inner side than at the upper side. In contrast, for the case of R_{ax} = 3.7 m, there is a thick divertor leg at both the upper and lower sides. Thick divertor legs are considered to carry a large number of particles and a large amount of energy. This change of heat load to different positions along the divertor legs by a small change of R_{ax} is used to decrease the peaked heat load. To examine this effect, thermocouples have been installed inside some divertor plates. Langmuir-probe electrodes have also been embedded in some plates in order to investigate the three-dimensional structure of the particle deposition pattern [23]. During long pulse operation, the temperature and particle flux profiles are measured by these detectors.

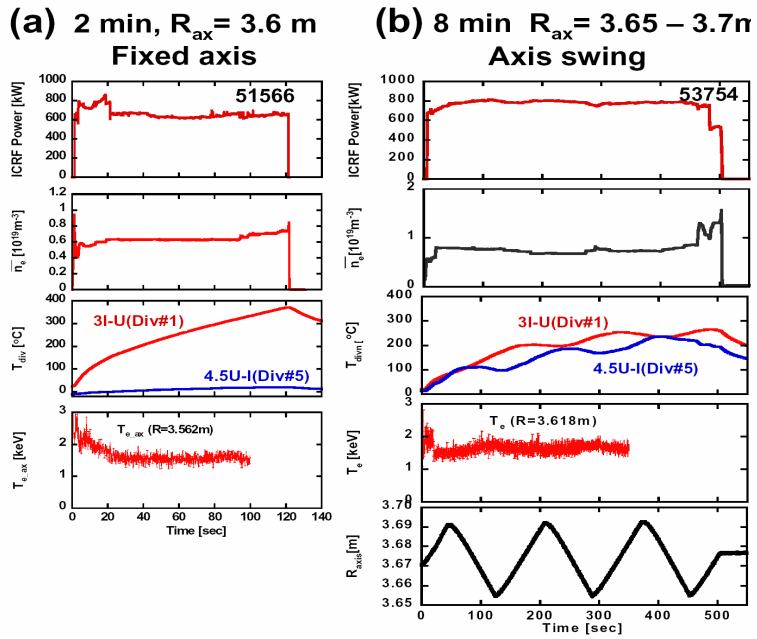

FIG. 6. Comparison between two discharges for the fixed-axis and swing-axis cases. (a) Temperature of one divertor plate in the fixed-axis case increases monotonically over 2 min, and then the plasma terminated. (b) In the swing-axis case, temperatures of plates stayed below 300 °C for a longer duration of 8 min.

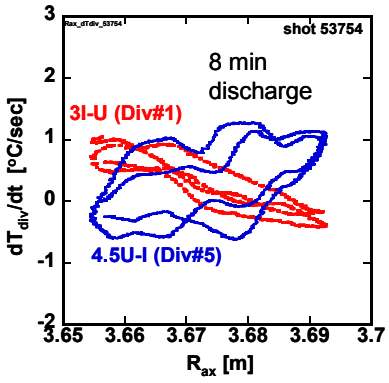

FIG. 7. Lissajous figures of the divertor heat load and magnetic axis radius are shown for the same plasma shown in FIG. 6(b). Div#1 and Div#5 show the out of phase relation.

In the 2004FY experimental program, an innovative technique was introduced: a real-time magnetic axis radius, R_{ax}, swing by controlling the vertical magnetic field. This technique successfully dispersed the divertor heat load along the divertor legs and also on each plate surface. This idea is based on an understanding of the LHD divertor physics mentioned above.

Figure 6 shows the comparison of two plasma discharges [24]. The left side shows the plasma parameters for the case of fixed R_{ax} operation (R_{ax} = 3.6 m), and the right figure shows the case for a discharge with R_{ax} swing (R_{ax} = 3.65–3.70 m). The input ICRF power and plasma density are almost the same in both cases. In the case of the fixed R_{ax} discharge, the temperature of the inner divertor plate increased monotonically during ICRF injection, and it reached approximately 400 °C after 120 s. The temperature of the top divertor plate remained low. On the other hand, in the discharge with R_{ax} swing, both the inner and top divertor plates were heated, but their temperatures did not monotonically increase. The heat load was reduced below the cooling capability of the carbon divertor plates for a period of 500 s.

During the R_{ax} swing operation, the temperatures of Div#1 and Div#5 changed almost out of phase with the frequency of the axis swing. The behavior of the divertor heat load can be investigated in terms of the temperature change of these tiles. Figure 7 shows a Lissajous figure using temperature derivatives of the two tiles and the magnetic axis radius for the discharge shown in Figure 6(b) during an 8 min operation discharge. In the figure, the heat load to Div#1 (inner-side tile) shows a monotonic dependence on the magnetic axis position, while the heat load to Div#5 (top-side tile) shows an inverse tendency. A somewhat early phase shift was observed in Div#5; the reason for this is not clear.

Using the R_{ax} swing technique, the particle deposition profile on one divertor tile was also effectively dispersed. Langmuir-probe arrays were embedded in several tiles, and the ion saturation current profile was measured [24]. The result shows that the axis swing also dispersed the particle flux on each divertor tile in a direction perpendicular to the leg traces. These results show that the R_{ax} swing technique is quite effective in dispersing the divertor heat load at both macroscopic (along the divertor plates array) and microscopic (on a divertor plate) levels. This new technique allowed us to achieve the long plasma sustainment time described in section II.

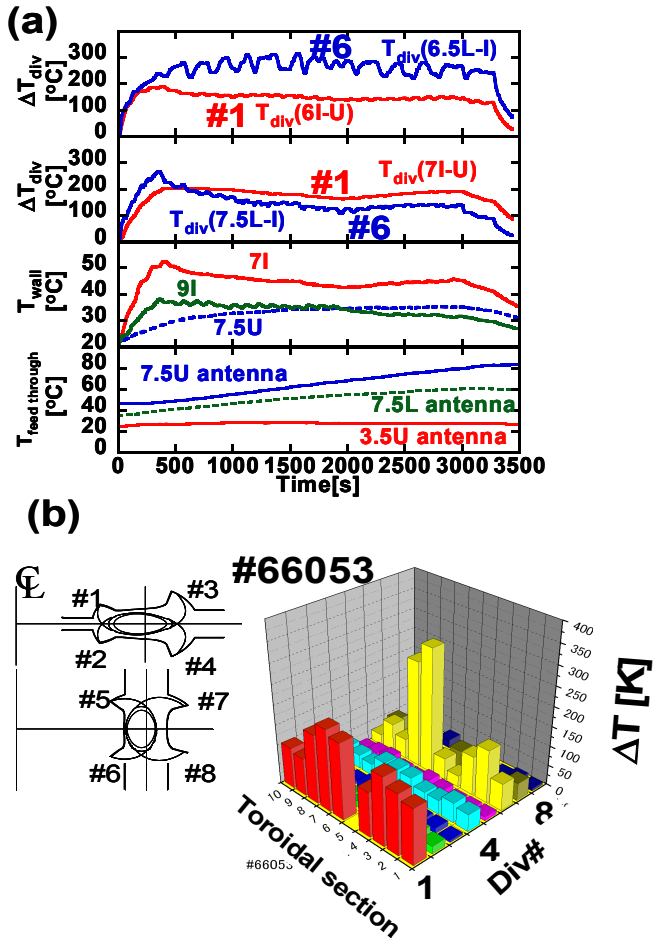

FIG. 8. Temporal behaviors of temperature in 54 min operation are shown. Temperatures of carbon plates in different divertor traces, stainless steel protector as the first wall and ICRF ceramic feedthrough section are shown in figure (a). Block chart (b) shows the temperature increment of sampled carbon divertor plates just at the end of the 54 min operation.

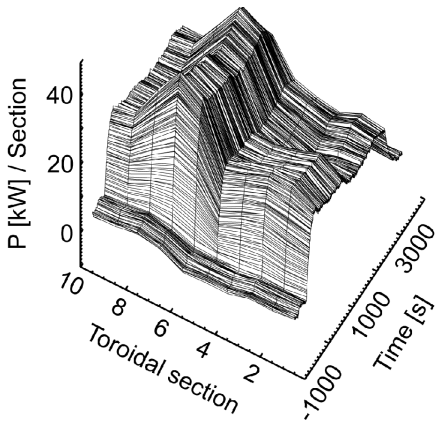

FIG. 9. Temporal and toroidal distribution of divertor channel power estimated from the temperature rises of the cooling water is shown in a 3 dimensional chart. Estimated power is the addition of the four divertor traces on each helical pitch.

4. Heat Load Distribution at the Steady State operation

Heat removal during a long operation time is an important issue in a steady state operation program. There are three kinds of heat sink in the LHD chamber. The main heat removal channel is the divertor structure consisting of carbon plates which are cooled by circulating water. The time evolutions of temperatures of four carbon plates for 54 min of operation are shown in Figure 8(a). Numerical analysis predicts that the plate of divertor numbers #1 and #6 have high heat loads from the core plasma through the scrape-off layer. The block graph (Fig. 8(b)) shows the temperature increment of the sampled carbon plates just after the 54 min operation. These graphs show that the maximum temperature increment stayed below 300 °C and that the peaked position was close to the ICRF antenna section. Another heat sink was the vacuum chamber wall which was also cooled by circulating water. The sampled temperatures of the stainless steel protector plates which cover the vacuum chamber as the first wall are also shown in Figure 8(a). The temperature increases of the wall are less than 30 °C, as shown in the figure.

The heat load to the divertor channel is not uniform as shown in the block chart of Figure 8. The heat load power to each divertor cooling channel can be estimated by the temperature increases of the cooling water at each toroidal section [9]. The estimated removed power distribution is plotted in the 3-D chart shown in Figure 9. The vertical axis indicates the removed power at each divertor channel and the horizontal axis indicates ten helical sections. The time trace is shown along the third axis (depth). ICRF antennas are located at the outward side of toroid in the helical sections 3.5 and 7.5. The apparent non-uniformity can be explained by the local heat loss near the antennas.

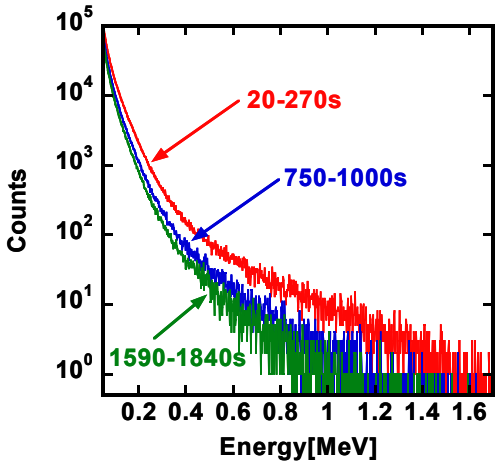

FIG. 10. High energy ion measurement by CXNPA during 54 min operation is shown. Flux counts are summed up during the indicated intervals.

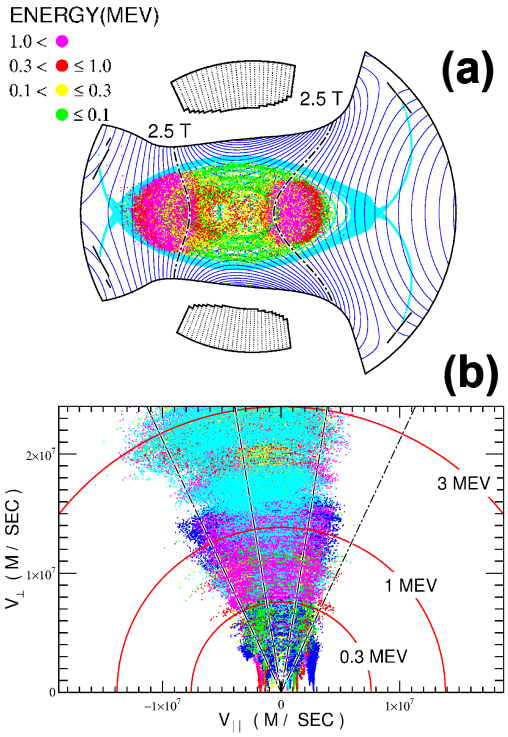

FIG. 11. (a) Poincare plot of calculated ICRF heated protons started with energy of 10 keV. Starting positions are at the cyclotron resonance layer nearest to the magnetic axis. (b) Poincare plots in parallel and perpendicular velocity plane is shown. (R_{ax} = 3.69 m, B=2.75T, E_{RF} = 20 kV/m, f = 38 MHz)

The portion of the divertor heat load power in relation to the injected ECH and ICRF power is estimated at about 40-50%. The heating efficiency defined by core heating power to injected power is roughly estimated at about 60-70%. Therefore, the remaining portion of around 20% of the injected power is lost by radiation and absorbed by the first wall.

5. High Energy Ion Production and Confinement Study

The long pulse operation of 54 min was performed mainly using the ICRF minority heating mode. The bulk plasma ion specie was helium and the minority ion specie was protons. During the operation, only helium gas was fed and no hydrogen gas was fed. Hydrogen ions were fed by wall outgas and recycling. Therefore, the minority proton ratio is not large during operation. Due to the low proton ratio, a high

energy ion tail was formed by ICRF heating in the LHD [12]. The high energy ion tail observed during the steady state operation is shown in Figure10. This is a time-integrated flux measured by a silicon diode NPA detector. The line of sight is on the equatorial plane and the detector is placed at the inward port. The high energy ion tail flux changed at different times as shown is Figure 10. The flux largely depends on the ICRF power. The heating power was gradually decreased to avoid arcing events. Therefore, the high energy particle flux decreased as the heating power decreased. The remarkable point here is that high energy particles beyond 1 MeV were produced and confined without any sign of confinement degradation in the high energy range. The maximum energy of the observed flux was 1.6 MeV when the heating ICRF power was around 600 kW with an ECH power of 110 kW.

The confinement ability of MeV-range particles in the LHD has been checked by analytic calculation [25]. Figure 11 shows the results of numerical calculation which includes full orbit calculation, RF acceleration, and finite LHD magnetic configuration without collisional process. Test particles started having an energy of 10 keV at the cyclotron resonance layers nearest to the magnetic axis. The calculation results show that particles of more than 1 MeV are produced and they remain as deeply trapped particles in the LHD's mirror sections (see Fig. 11(a)). The mirror section boundary is close to the cyclotron resonance layer as shown in the cross section of the LHD. The particles can be confined and are accelerated up to 3 MeV in the calculation. The accelerated and confined particles are plotted on the velocity space in Figure 11 (b). In this calculation, the magnetic axis radius is 3.69 m and this numerical calculation code predicts that the acceleration with the axis radius of 3.69 m is more efficient than that of 3.6 m which is the best confinement for bulk plasma in the LHD.

During the steady state operation seen in Figure 10, the magnetic axis was swept between Rax = 3.65 m and 3.67 m. The temporal change of the effective ion tail temperatures estimated in the energy range of 300-500 keV was plotted as the magnetic axis radius shown in Figure 12 as Lissajous figures. Figure 12(a) shows the case of the high ICRF heating power phase (sampled time is 30 - 300 sec in Fig.2) and (b) shows the case of the lower power phase (500 – 1500 sec in Fig.2). In both cases, the tail temperatures show a tendency to increase on the magnetic axis radius. This positive dependence is not the same with the bulk plasma properties. One possible reason for this is the difference in the acceleration process. The resonant cyclotron layers are located around the saddle point as shown in Figure 1 and the plasma core region is close to the resonant area in the case of a large magnetic axis.

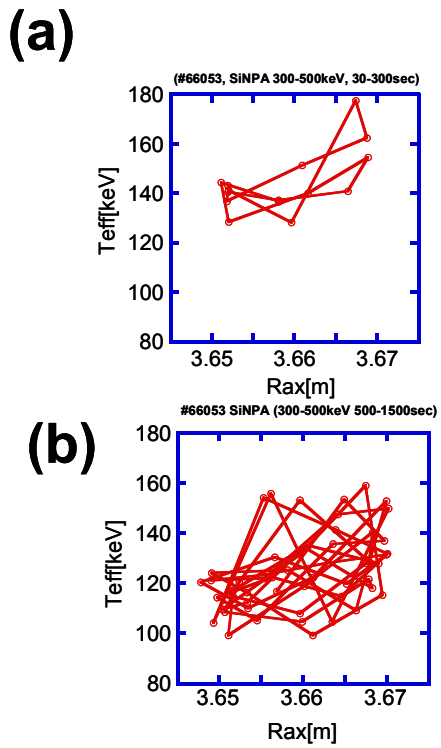

FIG. 12. The temporal change of the effective ion tail temperatures estimated in the energy range of 300-500 keV are plotted as the magnetic axis radius during the sampled time of (a) 30-300sec and (b) 500-1500 sec as the form of Lissajous figure.

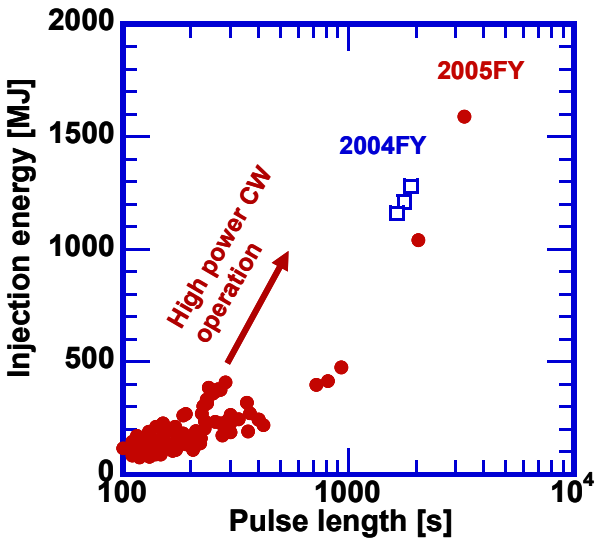

FIG. 13. Injected energies of long pulse operation in 2004FY and 2005FY are plotted versus plasma sustainment time. Next step of higher power operation is shown by arrow.

6. Summary

The long-pulse operation of a high-temperature plasma is one of the main topics regarding large fusion experimental devices. The long-duration discharges achieved in the LHD in the 2004FY and 2005FY programs [26] are plotted on the plane of total input energy and plasma-duration time in Figure 13. The 1.3 GJ energy of the LHD was the highest input energy for high-temperature plasmas at keV levels for any magnetic confinement device in the 2004FY program. In the 2005FY program, the LHD extended its own record to 1.6 GJ. The development of the new technology involving the swing divertor and the improvement of heating systems were key factors leading to this achievement. During the long operation time, high energy particles of over 1 MeV were detected and their properties were studied.

It should be remembered that the LHD is a heliotron-type device and does not require plasma current for confinement as do tokamaks. This accounts for the achievement of the long operation time. In addition, the plasma was heated and sustained mainly by the ICRF minority ion-heating mode, which produces high-energy ions that are easily trapped by magnetic field ripples. These results show that the heliotron configuration has a high potential as a steady-state fusion reactor.

Acknowledgment

The authors wish to thank the technical staff of the LHD group at the National Institute for Fusion Science for their helpful support during this work. This work was partially supported by NIFS budget code of NIFS05ULRR001, 504.

References

[1] O. Motojima, K. Akaishi, H. Chikaraishi, *et al.*, Nucl. Fusion 40, 599 (2000).
[2] O. Motojima, H. Yamada, A. Komori, *et al.*, Fusion Sci. Tech. 46, 1 (2004).
[3] S. Sudo, Y. Nagayama, M. Emoto, *et al.*, Rev. Sci. Instru. 72, 483 (2001).
[4] A. Komori, N. Ohyabu, H. Yamada, *et al.*, Plasma Phys. Control. Fusion 45, 671 (2003).
[5] S. Masuzaki, T. Morisaki, N. Ohyabu, *et al.*, Nucl. Fusion 42, 750 (2002).
[6] T. Morisaki, S. Masuzaki, M. Goto, *et al.*, Contrib. Plasma Phys. 42, 321(2002).
[7] N. Ohyabu, T. Watanabe, H. Ji, *et al.*, Nucl. Fusion 34, 387 (1994).
[8] T. Mutoh, R. Kumazawa, T. Seki, *et al.*, J. Plasma Fusion Res. 81, 229 (2005).
[9] Y. Nakamura, S. Masuzaki, T. Morisaki, H. Ogawa, T. Watanabe, Nucl. Fusion 46, 714–724(2006)
[10] S.Kubo, Y. Yoshimura, T. Shimozuma, *et al.*, AIP Conf. Proc. 16th Topiacal Conference on Radio Frequency Power in Plasmas, Park city, Utah, 2005, (American Institute of Physics, 2005) , AIP Conference Proceedings787, p.411.
[11] K. Ohkubo, S. Kubo, R. Kumazawa, *et al.*, Proc. of 20th IAEA Fusion Energy Conf., Vilamoura, Portugal, 2004, (IAEA, Vienna, 2004), IAEA-CN116/FT/P7-19.
[12] T. Mutoh, R. Kumazawa, T. Seki, *et al.*, Nucl. Fusion 43, 738 (2003).
[13] R. Kumazawa, T. Mutoh, T. Seki, *et al.*, Phys. Plasmas 8, 2139 (2001).
[14] D. van Houtte, G. Martin, A. Becoulet, *et al.*, Nucl. Fusion 44, L11 (2004).
[15] J. Pamela, E. R. Solano, JET EFDA Contrib., Nucl. Fusion 43, 1540 (2003).
[16] H. Zushi, K. Nakamura, K. Hanada, et al., Nucl. Fusion 45, S142 (2005).
[17] Ide H. et al 2004 Proc. 20th Int. Conf. on Fusion Energy (Vilamoura, 2004) (Vienna: IAEA) CD-ROM file OV/1-1 and http://www-naweb.iaea.org/napc/physics/fec/fec2004/datasets/index.html
[18] T. Mutoh, R. Kumzawa, T. Seki, *et al.*, Phys. Rev. Lett. 85, 4530 (2000).
[19] R. Kumazawa, T. Mutoh, T. Seki, *et al.*, J. Plasma Fusion Res. Ser. 3, 352 (2000).
[20] T. Seki, R. Kumazawa. T. Mutoh, *et al.*, J. Plasma Fusion Res. Ser. 5, 478 (2002).
[21] K. Saito, R. Kumazawa, T. Mutoh, *et al.*, Nucl. Fusion 41, 1021 (2001).
[22] Y. Takeiri, Y. Nakamura, N. Noda, *et al.*, Plasma Phys. Control. Fusion 42, 147 (2000).
[23] S. Masuzaki, T. Morisaki, M. Shoji, *et al.*, Fusion Science and Technology, Vol.50 pp.361-371 (2006)
[24] T. Mutoh, S. Masuzaki, R. Kumazawa, T. Seki, K. Saito, *et al*., Physics of Plasmas 13, 056118 (2006) DOI: 10.1063/1.2177204_
[25] T.Watanabe, Y.Matsumoto, M.Hishiki, et al., Nucl.Fusion, 46 291-305(2006) doi:10.1088/0029-5515/46/2/013
[26] R. Kumazawa, T. Mutoh, K. Saito, *et al.*, Nucl. Fusion 46 (2006) S13–S21